THE JOURNAL OF PHYSICAL CHEMISTRY Letters

Letter

pubs.acs.org/JPCL

# Voltage Dependent Charge Storage Modes and Capacity in Subnanometer Pores

Peng Wu,[†] Jingsong Huang,[‡] Vincent Meunier,[§] Bobby G. Sumpter,[‡] and Rui Qiao*[,†]

[†]Department of Mechanical Engineering, Clemson University, Clemson, South Carolina 29634-0921, United States

[‡]Center for Nanophase Materials Sciences and Computer Science and Mathematics Division, Oak Ridge National Laboratory, Bethel Valley Road, Oak Ridge, Tennessee 37831-6367, United States

[§]Department of Physics, Applied Physics, and Astronomy, Rensselaer Polytechnic Institute, Troy, New York 12180-3590, United States

Supporting Information

**ABSTRACT:** Using molecular dynamics simulations, we show that charge storage in subnanometer pores follows a distinct voltage-dependent behavior. Specifically, at lower voltages, charge storage is achieved by swapping co-ions in the pore with counterions in the bulk electrolyte. As voltage increases, further charge storage is due mainly to the removal of co-ions from the pore, leading to a capacitance increase. The capacitance eventually reaches a maximum when all co-ions are expelled from the pore. At even higher electrode voltages, additional charge storage is realized by counterion insertion into the pore, accompanied by a reduction of capacitance. The molecular mechanisms of these observations are elucidated and provide useful insight for optimizing energy storage based on supercapacitors.

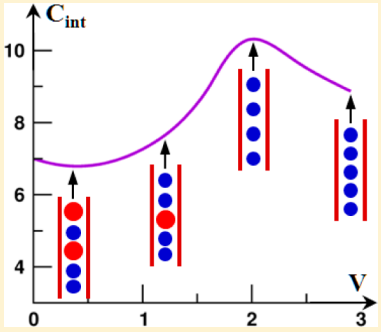


**SECTION:** Energy Conversion and Storage; Energy and Charge Transport

Supercapacitors continue to gain increasing attention as promising electrical energy storage systems with superior power density and excellent durability.[1,2] The principal limitation of supercapacitors, which store charge physically using the electrical double layers (EDLs) at electrode/electrolyte interfaces, is their modest energy density.[3,4] To enhance their energy density, diverse materials and electrolytes have been explored experimentally.[5−12] It was found that porous carbons featuring subnanometer pores hold great promise not only because of their large specific surface area but also due to their contribution to the anomalous increase in specific capacitance.[8,9] Meanwhile, room-temperature ionic liquids (RTILs) are well suited as electrolytes for supercapacitors mainly because of their wide electrochemical window.[11,12] To fully exploit the potential of subnanometer pores and RTILs in supercapacitors, a fundamental understanding of how charge storage in these materials depends on the EDL structures at the interface of carbon/RTILs, and on the operating conditions such as electrode voltage, must be obtained.

Numerous theoretical studies have been devoted to exploring the underlying physics for charge storage in subnanometer pores. The microstructure, capacitance, and dynamics in association with the EDLs in narrow pores and in RTILs have been extensively studied using analytical models, molecular dynamics (MD) simulations, and Monte Carlo (MC) simulations.[13−20] For example, Vatamanu et al. observed that the integral capacitance $C_{int}$ of nanopores can exceed that of flat electrodes.[21] Shim and Kim reported that $C_{int}$ of EDLs inside carbon nanotubes increases as the pore width of nanotubes decreases.[22] Skinner et al. developed a seminal model for the EDLs in nanopores and rationalized the observation of Vatamanu et al.[23] Kondrat et al. also showed that the differential capacitance $C_{diff}$ of micropores at zero electrode voltage increases as pore width reduces from ∼1.2 to ∼1.05 ion diameter.[24,25] They emphasized the role of image charge effects in determining the observed capacitance variation in different pores. More recently, we showed that the $C_{int}$ of nanopores filled with RTILs displays a richer behavior compared to that discovered earlier: while $C_{int}$ increases as pore width decreases in subnanometer pores, the opposite trend is found in slightly larger pores.[26] We attributed this phenomenon to the difference in "ionic solvation" inside these different pores. Our results were corroborated by those of Jiang et al.[27] and Feng and Cummings[28] published concurrently and showing that $C_{int}$ oscillates as pore width varies due to the interference of EDLs near the two opposing walls of each nanopore.

All these works have contributed significantly to the progress toward the elucidation of how pore width affects the charge storage in RTILs in subnanometer pores. On the other hand, only a limited number of theoretical studies have been devoted

**Received:** April 24, 2012
**Accepted:** June 12, 2012

   dx.doi.org/10.1021/jz300506j | J. Phys. Chem. Lett. 2012, 3, 1732−1737

to understand how operating conditions, which are critical design parameters of supercapacitors, affect charge storage in subnanometer pores. To date, only the variation of $C_{diff}$ of a pore filled with RTILs has been examined. On the basis of MC simulations,[25] Kondrat et al. showed that $C_{diff}$ is constant at low voltage and reaches a maximum at a certain voltage. At slightly higher voltages, $C_{diff}$ drops rapidly to zero. They "speculated that the peak in the capacitance *vs.* voltage curve is *related to* the 'complete filling' of the pore above a certain voltage" but no further mechanistic explanation of this behavior was provided.[25] Similar behavior was also observed by Skinner et al., although $C_{diff}$ did not rapidly drop to zero at larger voltages.[23] Likewise, they did not suggest a mechanistic explanation for the scenario that the pore is filled with RTILs at zero electrode voltage. Hence, the mechanisms of these important observations remain elusive.

In this work, we used MD simulations to examine the charge storage in a slit-shaped subnanometer pore in equilibrium with RTIL reservoirs. The pore that we studied has a center-to-center width of 0.78 nm. The pore walls are positively polarized. The polarizability was modeled within the framework of classical electrostatics to take into account image charge effects. Coarse-grained ion models were used (see Methods) with cations having the geometry of $DMI^+$ ions (widest dimensions in the imidazolium plane: ~0.57 × 0.8 nm) and anions having the geometry of $BF_4^-$ ions (diameter: ~0.52 nm). The ions studied herein are representative of a broad class of RTILs featuring asymmetric cation/anion sizes and complex shapes. Examination of the ion density profiles across the pore indicated that all cations and anions reside in the middle plane of the pore.

To quantify the charging of the pore as a function of the electrode voltage $\phi$, we first examine the occupancy of ions inside the pore by introducing an area-based number density $\rho_s$. Specifically, taking advantage of the fact that ions form a single layer inside the pore, we define $\rho_{s,+} = \int_0^W \rho_+(z)\, dz$, where $\rho_+(z)$ is the number density of cations across the pore, and $W$ is the pore width. $\rho_{s,-}$ is similarly defined. Essentially, $\rho_s$ represents the number of ions enclosed between the two parallel pore walls per unit area. Figure 1a shows the variation of $\rho_s$ for cations and anions as the electrode voltage increases. Using the data in Figure 1a, the pore wall surface charge densities $\sigma$, $C_{int}$, and $C_{diff}$ were computed and are shown in Figure 1b,c. These results indicate that the charge storage inside the pore examined here exhibits the following characteristics: (1) for $\phi$ < 1 V, charge storage is mainly achieved by swapping cations inside the pore with anions in the bulk electrolyte (hereafter referred to as ion-swapping), and both $C_{diff}$ and $C_{int}$ depend only weakly on the electrode voltage; (2) as electrode voltages increase further, additional charge storage inside the pore is achieved mainly by the removal of cations from the pore, and both $C_{int}$ and $C_{diff}$ increase (Both $C_{int}$ and $C_{diff}$ reach their maximum at ca. 1.7−2 V, close to the point at which cations are completely removed from the pore.); and 3) as the electrode voltage increases even further, more anions enter the pore and capacitance decreases. At $\phi \approx 2.89$ V, the steric limit of anion packing is not yet reached, and $C_{diff}$ is nonzero.

Some of the above observations are similar to those revealed in prior simulations and experimental studies. For example, the overall trend of $C_{diff}$ in Figure 1c, in particular, the existence of a potential $\phi_m$ at which $C_{diff}$ is maximized, is similar to those reported earlier by Skinner et al. and Kondrat et al.,[23,25] and closely resembles the trend reported in experimental characterization of capacitance of microporous electrodes featuring primarily 0.94 nm-wide pores in contact with 1-propyl-2,3-dimethylimidazolium bis(trifluoromethanesulfonyl)imide ($IM_{311}$-TFSI) RTIL.[29] However, our results also present key differences from prior theoretical works. For example, Figure 1c shows that, similar to that observed experimentally in ref 29 and theoretically in ref 23, $C_{diff}$ decreases moderately as voltages increases from $\phi_m$ to ~1.5$\phi_m$ as compared to the rapid decay of $C_{diff}$ toward zero reported in ref 25. In addition, in this work, as $\phi$ increases toward $\phi_m$, $C_{diff}$ increases rapidly, and the charge storage in the potential window 1 V < $\phi$ < 1.7 V is achieved mainly by the removal of co-ions from the pore with few counterions inserted. As $\phi$ increases beyond $\phi_m$, further charge storage is achieved by insertion of counterions into the pore. These observations contrast sharply with those reported in ref 25, in which charge storage at $\phi < \phi_m$ is governed by ion-swapping and extra counterion insertion, and charge storage at $\phi > \phi_m$ is entirely determined by ion-swapping. These

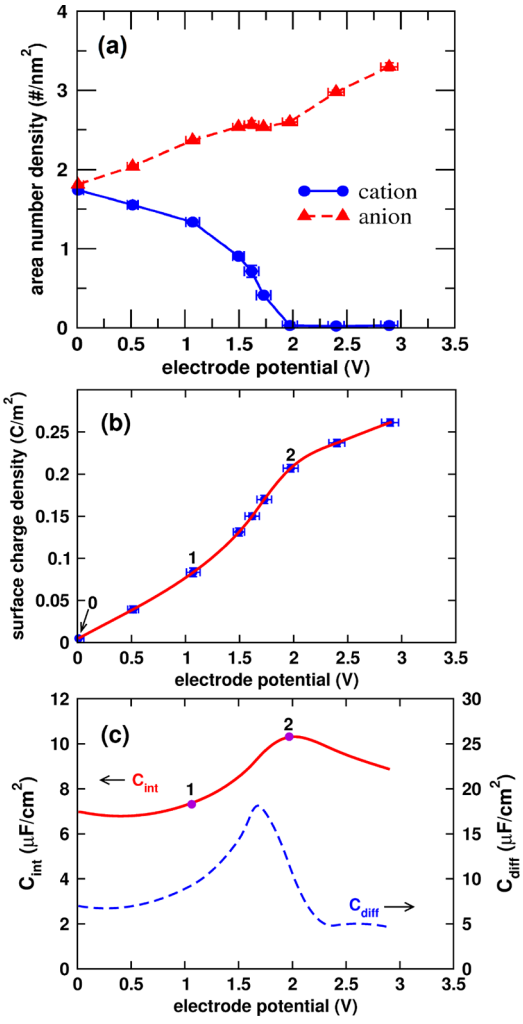


**Figure 1.** (a) Variation of the area-based number density, $\rho_s$, of cations and anions (see text for definition) as a function of the electrode voltage $\phi$. (b) Surface charge density, $\sigma$, of the slit pore walls as a function of the electrode voltage. The solid curve is a cubic spline interpolation of the MD data. (c) Variation of the integral and differential capacitance of the pore as a function of electrode voltage. The three state points 0, 1, and 2 discussed in the text have electrode voltages of $\phi$ = PZC, 1.07, and 1.97 V, respectively.


dx.doi.org/10.1021/jz300506j | *J. Phys. Chem. Lett.* 2012, 3, 1732−1737

differences highlight the rich behavior of charge storage in subnanometer pores.

Our analysis on mechanisms underlying the variation of modes of charge storage with electrode voltage focuses on $C_{int}$ instead of $C_{diff}$ since $C_{int}$ is the most important observable of supercapacitors. Also, we note that both $C_{int}$ and $C_{diff}$ show similar dependence on the electrode voltage in our system (cf. Figure 1c). To understand the evolving mode of charge storage inside the pore as a function of electrode voltage, consider a positively polarized electrode pore. As the voltage of the electrode increases by $\Delta\phi$, the pore wall surface charge density increases by $\Delta\sigma$, and the net charge inside the pore changes by $-\Delta\sigma$, which can be achieved in three possible modes: insertion of anions into the pore without removal of cations from the pore (i.e., pure anion insertion), removal of the cation from the pore without insertion of anion into the pore (i.e., pure cation removal), and insertion of anions into the pore accompanied by removal of the same amount of cations from the pore (i.e., ion swapping). Charge storage will proceed by one or several of these modes so that the system's free energy is minimized. We note two key features of the ion−ion interactions inside the system of Figure 1: (1) since all ions are distributed within a monolayer inside the pore, insertion or removal of ions strongly affect the separation between ions (especially for ions with the same charge) already inside the pore, and (2) ion−ion interactions are screened by polarizable pore walls and decrease (increase) exponentially as the ion−ion separation in the plane parallel to the pore walls increases (decreases).[23,25] To examine the energetics of ion−ion interactions inside a pore as it becomes charged, note that the insertion of anions into the pore tends to increase the system's energy by reducing the anion−anion separations inside the pore (thus enhancing their repulsion), but this is partially offset by the increased cation−anion attraction. Removal of cations from the pore tends to increase the system's energy by reducing anion−cation attractions, but this is offset by a reduction of cation−cation repulsions and anion−anion repulsions (anion−anion separation increases as the removal of cations leaves space for anions).

At low electrode voltage ($\phi$ < 1.0 V), the number of anions and cations inside the pore does not differ significantly. As the electrode voltage increases by $\Delta\phi$, the change of the system's energy after inserting an anion into the pore is similar to that after removing a cation from the pore. Therefore, the system does not exhibit notable preference between anion insertion and cation removal. As such, charge storage is realized by simultaneous insertion of anions and removal of cations, i.e., ion swapping. Since each removed cation leaves more space than that occupied by each inserted anion, a small amount of net anion insertion is also observed in Figure 1a. As the electrode voltage increases to higher values (1.0 V < $\phi$ < 1.97 V), the pore is filled with more anions than cations (e.g., the ratio of $\rho_{s,-}/\rho_{s,+}$ is 2.82 at $\phi$ = 1.50 V). In such a situation, inserting anions will reduce anion−anion separation and sharply increase anion−anion repulsion (recall ion−ion interactions increase exponentially as their separation decreases). Meanwhile, the enhancement of cation−anion attraction is moderate as cations inside the pore are already surrounded by many anions, and the newly inserted anions are located at a position away from the cation and contribute little to cation−anion attraction. On the other hand, removing bulky cations from inside the pore leaves larger spaces for the anions inside the pore and greatly reduces their repulsion, even though the cation−anion attraction is also reduced. Since the overall energetics of the system at large voltage is dominated by anion−anion repulsions, removing cations is more favorable than inserting anions. As a result, the additional charge storage inside the pore is achieved predominantly by cation removal when the electrode voltage increases. Such a trend is particularly clear at high electrode voltages (e.g., $\phi$ > 1.5 V), where additional charge storage as the electrode voltage increases is nearly exclusively achieved by cation removal. As electrode voltage increases beyond $\phi \approx$ 1.97 V, all cations are removed from the pore and additional charge storage is achieved by anion insertion. Clearly, the mode of charging at moderate electrode voltages revealed here, i.e., the predominance of cation removal as voltage increases from 1 to 2 V, is related to the asymmetry of cation and anion sizes. Since the sizes of cations and anions in ref 25 are exactly the same, the different modes of charging found in this work and in ref 25 are likely caused by the different ions studied.

To understand the variations of $C_{int}$ as a function of the electrode voltage $\phi$, we use a model we developed in a previous work. As shown in ref 26, by neglecting the cavity energy and entropic effects, the scale of $C_{int}$ of a nanopore follows

$$C_{int} \sim \frac{e}{-\Delta E^{elec}_{i\to ions}(0 \to \sigma)/z_i\sigma} \quad (1)$$

where $z_i$ is ion $i$'s valence, and $\Delta E^{elec}_{i\to ions}(0\to\sigma) = E^{elec}_{i\to ions}(\sigma) - E^{elec}_{i\to ions}(0)$ is the change of ion $i$'s energy due to its electrostatic interactions with ions inside a pore as the surface charge density of the pore increases from 0 to $\sigma$ under the action of an electrical potential. Note that eq 1 is valid only if the cavity energy and entropy effects can be neglected when they are smaller than the change of the ion's electrostatic energy as the pore walls are electrified. As will be shown later, such a condition is met for electrode voltages smaller than 2 V but not for higher voltages. Equation 1 is applicable to both cations and anions. Essentially, eq 1 correlates the capacitance of a pore with the *variation* of electrostatic ion energy as the pore becomes electrified. To understand eq 1, consider a neutral pore. As the electrical potential on the pore wall increases from potential of zero charge (PZC) to $\phi$, removal of a cation $i$ from the pore is affected by (1) the increase in electrode potential, which tends to drive cation $i$ out of the pore, (2) the decrease in net ionic charge inside the pore, which creates an increased attraction (hereafter referred to as ionic attraction) to cation $i$ and hinders its removal. Consequently, for each unit of positive charge the pore wall gains (or, each unit of negative ionic charge the pore gains), if the attraction rendered by ions inside the pore to cations increases weakly (i.e., $-\Delta E^{elec}_{+\to ions}(0\to\sigma)/\sigma$ is small), it will be easy to remove a large amount of cations from the pore at a given $\phi$, which tends to lead to large $C_{int}$. Similar interpretation applies to anions.

Equation 1 can be used to understand the variations of $C_{int}$ for $\phi$ < 1.97 V. We can apply this equation to the cations since cation removal plays a key role for the charge storage inside the pore with a wall potential of $\phi$ < 1.97 V. Figure 2 shows the variation of $-\Delta E^{elec}_{+\to ions}(0\to\sigma)/\sigma$ for $\phi$ < 1.97 V. We observe that, as $\phi$ increases from 0.5 to 1.97 V, $-\Delta E^{elec}_{+\to ions}(0\to\sigma)/\sigma$ decreases by 27%. According to eq 1, $C_{int}$ should increase by ~36% in this potential window, as compared to the 50% increase observed in Figure 1c. The good agreement confirms that, for $\phi$ < 1.97 V, eq 1 is valid (i.e., the cavity energy and entropy effects can be neglected when studying the trend of capacitance variation) and the larger $C_{int}$ at higher $\phi$ is mainly caused by the smaller $-\Delta E^{elec}_{+\to ions}(0\to\sigma)/\sigma$ at higher $\phi$. This


dx.doi.org/10.1021/jz300506j | J. Phys. Chem. Lett. 2012, 3, 1732−1737

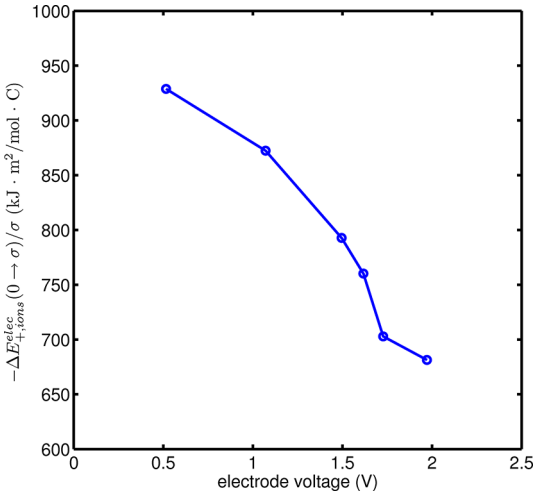


**Figure 2.** Variation of $-\Delta E^{\mathrm{elec}}_{+\rightarrow \mathrm{ions}}(0 \rightarrow \sigma)/\sigma$ as a function of the electrode potential on the pore wall.

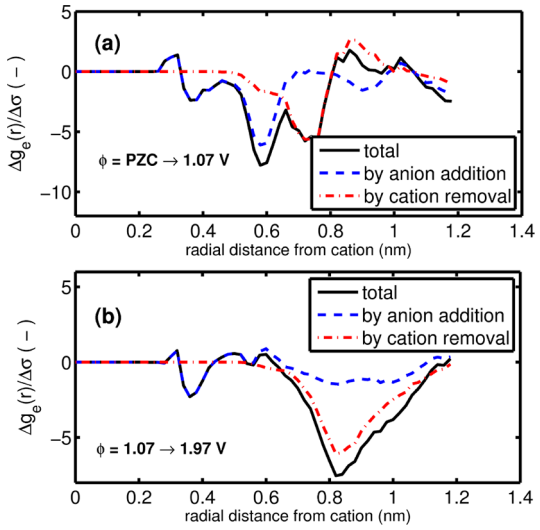


**Figure 3.** Change of the ionic charge distribution function of the cations inside the pore ($\Delta g_e(r) = g_e(r)|_{\phi 2} - g_e(r)|_{\phi 1}$) as the electrode voltage on the pore wall increases from ~0 to 1.07 V (a) and from 1.07 V to 1.73 V (b). Contributions to $\Delta g_e(r)$ by the addition of anions to the vicinity of cation and by the removal of cations from the vicinity of cations are also shown. To facilitate the comparison of $\Delta g_e(r)$ in these two cases, $\Delta g_e(r)$ is scaled by change of the pore wall surface charge density $\Delta\sigma$ in each potential window.

behavior can be understood by examining the ionic charge distribution near cations at different $\phi$. To illustrate this, we show in the following why $-\Delta E^{\mathrm{elec}}_{+\rightarrow \mathrm{ions}}(0\rightarrow\sigma)/\sigma$ at $\phi$ = 1.97 V is smaller than that at $\phi$ = 1.07 V. Let us first define three state points 0, 1, and 2 (cf. Figure 1b) corresponding to slit pores held at $\phi$ = PZC, 1.07, and 1.97 V. We next note that $-\Delta E^{\mathrm{elec}}_{+\rightarrow \mathrm{ions}}(0\rightarrow\sigma_2)/\sigma_2 < -\Delta E^{\mathrm{elec}}_{+\rightarrow \mathrm{ions}}(0\rightarrow\sigma_1)/\sigma_1$ is mathematically equivalent to $-\Delta E^{\mathrm{elec}}_{+\rightarrow \mathrm{ions}}(\sigma_1\rightarrow\sigma_2)/(\sigma_2 - \sigma_1) < -\Delta E^{\mathrm{elec}}_{+\rightarrow \mathrm{ions}}(0\rightarrow\sigma_1)/\sigma_1$, where $\sigma_1$ and $\sigma_2$ correspond to $\phi_1$ = 1.07 V and $\phi_2$ = 1.97 V. The latter is the net result of two factors: (1) the different modes of charge storage in the potential window $\phi$ < 1.07 and 1.07 V < $\phi$ < 1.97 V and (2) the rapid decay of the ion−ion interactions inside the present pore as their separation increases. Specifically, as $\phi$ increases from PZC to 1.07 V, anions (cations) enter (leave) the pore. During this process, the energy of a cation inside the pore becomes more negative because it is "effectively" surrounded by a larger number of negative ionic charges, which originates either from packing of more anions or removal of cations near the cation. Since a cation's energy depends on the ionic charges near it, we quantify the ionic charges near each cation inside the pore by defining an ionic charge distribution function $g_e(r)$ in the spirit of the radial distribution function: $g_e(r) = (\rho_{s,+}(r) - \rho_{s,-}(r))e$, where $\rho_{s,+}(r)$ and $\rho_{s,-}(r)$ are the average local area-based number densities of cation and anions at distance $r$ from each cation inside the pore, and $e$ is the unit charge. The change of the ionic charge distribution function of cations inside the pore $\Delta g_e(r)$ as the electrode voltage varies is shown in Figure 3a,b. Figure 3a shows that, as $\phi$ increases from PZC to 1.07 V, the increased "effective" negative ionic charge near each cation inside the pore is mainly due to insertion of anions at a distance of 0.5−0.65 nm from it and the removal of cations at a distance of 0.6−0.8 nm from it. As $\phi$ increases from 1.07 to 1.97 V, few anions enter the pore, but many cations leave the pore. During this process, the energy of each cation that remained inside the pore also becomes more negative because it is surrounded by more negative ionic charges. However, these negative ionic charges originate mostly from the removal of cations near the remaining cations. Since the separation of cations inside the pore is large at 1.07 V, cations are removed at distances far from where the cations remained in the pore. Indeed, Figure 3b shows that, as $\phi$ increases from 1.07 to 1.97 V, the increased "negative" ionic charges near each cation inside the pore is mostly due to the removal of cations from a distance 0.7 to 1.2 nm from it. Hence, per each unit surface charge density the pore wall gains, although the increase of the negative ionic charge near the cations remained inside the pore is the same for the two potential windows, these effective negative ionic charges are distributed closer to the cation in the first potential window. Since the interactions between these effective charges and the cations that remained inside the pore decays rapidly as their separation increases, it follows that $-\Delta E^{\mathrm{elec}}_{+\rightarrow \mathrm{ions}}(\sigma_1 \rightarrow \sigma_2)/(\sigma_2 - \sigma_1)$ is smaller than $-\Delta E^{\mathrm{elec}}_{+\rightarrow \mathrm{ions}}(0 \rightarrow \sigma_1)/\sigma_1$, and $C_{\mathrm{int}}$ at 1.97 V is larger than that at 1.07 V.

Equation 1, however, cannot easily account for the decrease of $C_{\mathrm{int}}$ as $\phi$ increases beyond 1.97 V. Specifically, since anion insertion dominates the increased charge storage as $\phi$ increases beyond 1.97 V, we computed the variation of $-\Delta E^{\mathrm{elec}}_{+\rightarrow \mathrm{ions}}(0 \rightarrow \sigma)/\sigma$ for 1.97 V ≤ $\phi$ ≤ 2.98 V and found that it remains essentially constant. Thus, eq 1 predicts $C_{\mathrm{int}}$ to be a constant in this potential window, while Figure 1c indicates that $C_{\mathrm{int}}$ decreases as $\phi$ increases. The decrease of $C_{\mathrm{int}}$ for this potential window is likely caused by entropic effects that are neglected in eq 1. For $\phi$ > 1.97 V, the area-based number density of ions inside the pore increases as $\phi$ increases (cf. Figure 1a), which tends to reduce the entropy per unit area. Such an effect becomes more and more important as $\phi$ increases and tends to hinder the insertion of additional anions into the pore, thereby reducing $C_{\mathrm{int}}$.

In summary, we utilized MD simulations to determine how charge storage inside a subnanometer pore in equilibrium with an RTIL reservoir depends on the electrode voltage. We showed that, at lower voltages, charge storage of the pore is achieved by swapping co-ions in the pore with counterions in the RTIL reservoir. As voltage increases, additional charge storage is due mainly to the removal of co-ions from the pore, and capacitance increases as a function of the electrode voltage. This change of charge storage mode is caused by the asymmetry in size of the counterions and co-ions and by the


dx.doi.org/10.1021/jz300506j | J. Phys. Chem. Lett. 2012, 3, 1732−1737

fact that, at high potential, the counterion/counterion repulsion dominates the system's energy. It follows that the removal of co-ions is more effective in reducing this energy than the insertion of counterions. The capacitance increases because, at higher potential, the stabilization of co-ions inside the pore by the ionic charges inside the pore per unit surface charge on the pore wall becomes weaker, which is in turn caused by the short-ranged nature of the electrostatic interactions in subnanometer pores. At even higher electrode voltage, additional charge storage is realized by counterion insertion into the pore, and the capacitance decreases due to entropic effects. These results illustrate that the charge storage in subnanometer pores exhibits rich behaviors as the voltage changes. The various trends depend on the specific nature of RTILs (e.g., cation/anion size asymmetry) and the generic features of subnanometer pores (e.g., short-ranged electrostatic interactions). Clearly, harnessing this behavior could be useful for improving the performance of supercapacitors.

## METHODS

The MD simulations were performed using a customized version of the package Gromacs.[30] The MD system consists of an electrode featuring a slit pore and a RTIL reservoir in direct contact with the electrode (see Figure S1 in the Supporting Information). The dimensions of the slit pore and RTIL reservoir, detailed in the Supporting Information, were chosen so that the effects associated with the slit pore entrance do not affect the ion density profile in the pore interior. The electrical polarizability of the electrode and the pore surfaces is modeled using the method developed in ref 31. The force fields for cation and anion were taken from ref 26. The geometry of ions is shown in Figure S1. The net charge of each ion is localized on one of its atoms (see Figure S1). These force fields have been found to predict properties of EDLs well compared to fully detailed force fields.[28] We confirmed that distributing the net charge of each ion evenly on its constituent atoms does not change the trends reported here. Simulations were performed in the NVT ensemble ($T$ = 400 K). Each system was simulated three times using different initial configurations, and each simulation consisted of an equilibrium run of 20 ns and a production run of 20 ns. Details of the simulation techniques and calculation of pore surface charge/potential are summarized in the Supporting Information.

## ASSOCIATED CONTENT

### Supporting Information

A schematic of the MD system, details of the MD setup, and simulation techniques. This material is available free of charge via the Internet at http://pubs.acs.org.

## AUTHOR INFORMATION

### Corresponding Author

*E-mail: rqiao@clemson.edu. Web: http://www.clemson.edu/~rqiao.

### Notes

The authors declare no competing financial interest.

## ACKNOWLEDGMENTS

The authors thank the Clemson-CCIT office for providing computer time. R.Q. acknowledges support from the NSF under Grant No. CBET-0967175. R.Q. and V.M. were partially supported by an appointment to the HERE program for faculty at the Oak Ridge National Laboratory (ORNL) administered by ORISE. The authors at ORNL acknowledge the support from the Center for Nanophase Materials Sciences, which is sponsored at ORNL by the Scientific User Facilities Division by the Office of Basic Energy Sciences, U.S. Department of Energy. We also acknowledge computational support from the National Center for Computational Sciences and Oak Ridge Leadership Computing Facility.

## REFERENCES

(1) Miller, J. R.; Simon, P. Materials Science - Electrochemical Capacitors for Energy Management. *Science* **2008**, *321*, 651−652.
(2) Simon, P.; Gogotsi, Y. Materials for Electrochemical Capacitors. *Nat. Mater.* **2008**, *7*, 845−854.
(3) Conway, B. E. *Electrochemical Supercapacitors*; Kluwer Academic: New York, 1999.
(4) Dunn, B.; Kamath, H.; Tarascon, J.-M. Electrical Energy Storage for the Grid: A Battery of Choices. *Science* **2011**, *334*, 928−935.
(5) Zhu, Y.; Murali, S.; Stoller, M. D.; Ganesh, K. J.; Cai, W.; Ferreira, P. J.; Pirkle, A.; Wallace, R. M.; Cychosz, K. A.; Thommes, M.; et al. Carbon-Based Supercapacitors Produced by Activation of Graphene. *Science* **2011**, *332*, 1537−1541.
(6) Centeno, T. A.; Stoeckli, F. The Volumetric Capacitance of Microporous Carbons in Organic Electrolyte. *Electrochem. Commun.* **2012**, *16*, 34−36.
(7) Raymundo-Piñero, E.; Kierzek, K.; Machnikowski, J.; Béguin, F. Relationship between the Nanoporous Texture of Activated Carbons and Their Capacitance Properties in Different Electrolytes. *Carbon* **2006**, *44*, 2498−2507.
(8) Largeot, C.; Portet, C.; Chmiola, J.; Taberna, P.-L.; Gogotsi, Y.; Simon, P. Relation between the Ion Size and Pore Size for an Electric Double-Layer Capacitor. *J. Am. Chem. Soc.* **2008**, *130*, 2730−2731.
(9) Chmiola, J.; Yushin, G.; Gogotsi, Y.; Portet, C.; Simon, P.; Taberna, P. L. Anomalous Increase in Carbon Capacitance at Pore Sizes Less Than 1 Nanometer. *Science* **2006**, *313*, 1760−1763.
(10) Baldelli, S. Surface Structure at the Ionic Liquid-Electrified Metal Interface. *Acc. Chem. Res.* **2008**, *41*, 421−431.
(11) Ohno, H. *Electrochemical Aspects of Ionic Liquids*, 2nd ed.; John Wiley & Sons: Singapore, 2011.
(12) Sato, T.; Masuda, G.; Takagi, K. Electrochemical Properties of Novel Ionic Liquids for Electric Double Layer Capacitor Applications. *Electrochim. Acta* **2004**, *49*, 3603−3611.
(13) Bazant, M. Z.; Storey, B. D.; Kornyshev, A. A. Double Layer in Ionic Liquids: Overscreening versus Crowding. *Phys. Rev. Lett.* **2011**, *106*, 046102.
(14) Wander, M. C. F.; Shuford, K. L. Molecular Dynamics Study of Interfacial Confinement Effects of Aqueous NaCl Brines in Nanoporous Carbon. *J. Phys. Chem. C* **2010**, *114*, 20539−20546.
(15) Feng, G.; Jiang, D.-E.; Cummings, P. T. Curvature Effect on the Capacitance of Electric Double Layers at Ionic Liquid/Onion-like Carbon Interfaces. *J. Chem. Theory Comput.* **2012**, *8*, 1058−1063.
(16) Singh, R.; Monk, J.; Hung, F. R. Heterogeneity in the Dynamics of the Ionic Liquid [BMIM$^+$][ $PF_6^-$] Confined in a Slit Nanopore. *J. Phys. Chem. C* **2011**, *115*, 16544−16554.
(17) Vatamanu, J.; Cao, L. L.; Borodin, O.; Bedrov, D.; Smith, G. D. On the Influence of Surface Topography on the Electric Double Layer Structure and Differential Capacitance of Graphite/Ionic Liquid Interfaces. *J. Phys. Chem. Lett.* **2011**, *2*, 2267−2272.
(18) Vatamanu, J.; Borodin, O.; Smith, G. D. Molecular Insights into the Potential and Temperature Dependences of the Differential Capacitance of a Room-Temperature Ionic Liquid at Graphite Electrodes. *J. Am. Chem. Soc.* **2010**, *132*, 14825−14833.
(19) Merlet, C.; Rotenberg, B.; Madden, P. A.; Taberna, P.-L.; Simon, P.; Gogotsi, Y.; Salanne, M. On the Molecular Origin of Supercapacitance in Nanoporous Carbon Electrodes. *Nat. Mater.* **2012**, *11*, 306−310.
(20) Merlet, C.; Salanne, M.; Rotenberg, B; Madden, P. A. Imidazolium Ionic Liquid Interfaces with Vapor and Graphite:

Interfacial Tension and Capacitance From Coarse-grained Molecular Simulations. *J. Phys. Chem. C* **2011**, *115*, 16611−16618.
(21) Vatamanu, J.; Borodin, O.; Smith, G. D. Molecular Dynamics Simulations of Atomically Flat and Nanoporous Electrodes with a Molten Salt Electrolyte. *Phys. Chem. Chem. Phys.* **2010**, *12*, 170−182.
(22) Shim, Y.; Kim, H. J. Nanoporous Carbon Supercapacitors in an Ionic Liquid: A Computer Simulation Study. *ACS Nano* **2010**, *4*, 2345−2355.
(23) Skinner, B.; Chen, T. R.; Loth, M. S.; Shklovskii, B. I. Theory of Volumetric Capacitance of an Electric Double-Layer Supercapacitor. *Phys. Rev. E* **2011**, *83*, 056102.
(24) Kondrat, S.; Kornyshev, A. Superionic State in Double-Layer Capacitors with Nanoporous Electrodes. *J. Phys.: Condens. Matter* **2011**, *23*, 022201.
(25) Kondrat, S.; Georgi, N.; Fedorov, M. V.; Kornyshev, A. A. A Superionic State in Nano-porous Double-Layer Capacitors: Insights from Monte Carlo Simulations. *Phys. Chem. Chem. Phys.* **2011**, *13*, 11359−11366.
(26) Wu, P.; Huang, J.; Meunier, V.; Sumpter, B. G.; Qiao, R. Complex Capacitance Scaling in Ionic Liquids-Filled Nanopores. *ACS Nano* **2011**, *5*, 9044−9051.
(27) Jiang, D. E.; Jin, Z. H.; Wu, J. Z. Oscillation of Capacitance inside Nanopores. *Nano Lett.* **2011**, *11*, 5373−5377.
(28) Feng, G.; Cummings, P. T. Supercapacitor Capacitance Exhibits Oscillatory Behavior as a Function of Nanopore Size. *J. Phys. Chem. Lett.* **2011**, *2*, 2859−2864.
(29) Kondrat, S.; Perez, C. R.; Presser, V.; Gogotsi, Y.; Kornyshev, A. A. Effect of Pore Size and Its Dispersity on the Energy Storage in Nanoporous Supercapacitors. *Energy Environ. Sci.* **2012**, *5*, 6474−6479.
(30) Lindahl, E.; Hess, B.; van der Spoel, D. Gromacs 3.0: A Package for Molecular Simulation and Trajectory Analysis. *J Mol. Model.* **2001**, *7*, 306−317.
(31) Raghunathan, A. V.; Aluru, N. R. Self-Consistent Molecular Dynamics Formulation for Electric-Field-Mediated Electrolyte Transport through Nanochannels. *Phys. Rev. E* **2007**, *76*, 011202.